Research Article

Yan-Shuang Yang*, Meng-Yu Yin, Zhan-Rong Zhang, Si-Pei Cheng, and Jia-Wen Hou

DEM study on the loading rate effect of marble under different confining pressures

https://doi.org/10.1515/rams-2023-0121 received April 24, 2023; accepted September 08, 2023

Abstract: Based on the conventional triaxial compression test of marble, the microscopic parameters corresponding to the macroscopic mechanical properties of marble were obtained by PFC2D, and on this basis, discrete element method models were established to conduct numerical tests of triaxial compression of marble under different confining pressures and loading rates to study the effect of loading rates on the rock specimens. Under the same confining pressure, brittle damage occurs in marble when the loading rate is low, and the damage type transforms from brittle to ductile as the loading rate increases. The peak strength, cracking stress, damage stress, cohesion, and internal friction angle of marble appear to increase with the increase in the loading rate under the same confining pressure. The characteristic stresses and strength parameters are linearly related to the loading rate. The influence of the loading rate on the peak strength is the most significant. With the increase in the confining pressure, the fitting coefficient of the linear relationship between initiation stress and loading rate decreases from 18.9 to 15.4 for different confining pressures, indicating that the growth rate of initiation stress decreases with the increase in the confining pressure when the loading rate is increased, and the increase in confining pressure suppresses the growth rate of initiation stress with loading rate.

Keywords: marble, particle flow simulation, triaxial compression, strength parameter, characteristic stress

Meng-Yu Yin, Si-Pei Cheng, Jia-Wen Hou: Key Laboratory of Intelligent Health Perception and Ecological Restoration of Rivers and Lakes, Ministry of Education, Hubei University of Technology, Wuhan 430068, China

Zhan-Rong Zhang: China Railway Siyuan Survey and Design Group Co., Ltd, Wuhan, Hubei 430063, China

1 Introduction

In recent years, with the degree of exploitation of underground space and the increasing demand for renewable energy in China, more complex rock mechanics problems have arisen in constructing large hydropower stations and their main structures. For example, during the construction of the underground engineering of hydropower, the *in situ* stress will change and cause the deformation of the surrounding rock [1–3]. The surrounding rock gradually accumulates damage during the loading process. When the exterior load exceeds a certain level, the rock is damaged, its strength is reduced, and in severe cases, the surrounding rock is destroyed and destabilized [4,5]. After the excavation of underground projects, a high-ground stress environment is often formed, and the mechanical parameters of the deep rock body deteriorate [6–8].

When changing the loading rate, the mechanical properties of the rock change, which is called the loading rate effect. The rock loading rate effect is one of the crucial causes of various dynamic hazards in the development of underground space and resources [9–11]. Changing the loading rate will affect the stress distribution, displacement distribution, deformation damage characteristics, and energy storage and dissipation of the engineering rock under the excavation load, affecting the stability of the surrounding rock. The loading rate effect has even more significant impact on hard brittle rocks [12,13]. Therefore, the loading rate effect of deep rock masses under different confining pressures is of important research significance.

The study of loading rate effect was carried out by conducting laboratory tests under different stress paths, with construction environment and rock type as variables. Jiang *et al.* [14] changed the loading rate of shale in uniaxial compression tests, detected the acoustic emission energy of rock specimens during the loading process, and calculated the critical index by the maximum likelihood estimation method to analyze the critical failure actions of rock specimens. Qin *et al.* [15] carried out lateral compression tests on crushed vein rocks at different loading rates and combined the energy characteristics of rocks in acoustic

^{*} Corresponding author: Yan-Shuang Yang, Key Laboratory of Intelligent Health Perception and Ecological Restoration of Rivers and Lakes, Ministry of Education, Hubei University of Technology, Wuhan 430068, China, e-mail: y1y1s1@qq.com

emission and the crushing process of particles in numerical tests to obtain the deformation mechanism of coal gangue under compression. Zhao *et al.* [16] discussed the elastic energy, dissipation energy, and damage variables of rocks during the change in stress–strain curve by conducting uniaxial compression tests on brittle granite at different loading rates. Moreover, damage variables obtained from the stress–strain curve and the damage characteristics of the rock from the perspective of energy evolution were studied and compared. Li *et al.* [17] conducted uniaxial compression tests under different loading rates on original rock samples and rock samples containing initial damage to investigate the effects of loading rate and initial damage on the energy evolution characteristics.

Loading rate effect is mostly studied by uniaxial compression tests, and the effect of rate on the mechanical properties of rocks under different confining pressures is less studied.

Due to the limitation of test equipment and testing means, monitoring the continuous phenomenon during the stressing process of rock specimens in laboratory tests is difficult. It is difficult to obtain the crack initiation, extension, and penetration inside the sample, which cannot reveal the loading rate effect of the rock from the microscopic level during the loading process [18,19]. There are also limitations in the simulation of complex mechanical environments. Therefore, the loading rate effects of rock samples in different stress paths need to be studied based on laboratory tests combined with numerical simulation techniques.

Discrete element method (DEM) has special advantages in obtaining crack propagation, damage accumulation, stress adjustment, and dynamic procedure of test and microscopic destruction in rock specimen, which has been widely used to study the micro behaviors of granular materials. Therefore, DEM is a powerful complement to conventional laboratory tests and numerical simulations based on the finite element method [20-24]. Kim et al. [25] conducted numerical tests of uniaxial compression and Brazilian splitting under different loading rates on granite by DEM model to quantitatively analyze the effects of loading rate on stress-strain, fracture morphology, and energy conversion during damage. Zhou et al. [26] established a numerical model by PFC3D and carried out compression tests under 10 MPa confining pressure to obtain the evolution of axial stress and the number of cracks in simulated rock specimens under different axial loading rates. The laboratory tests with loading rate effect as research object is difficult to carry out. Numerical tests make up for the limitations of laboratory tests and reflect the scientific principles easily and comprehensively.

DEM is used as the primary research tool to obtain the effect of loading rate on the strength parameters and characteristic stresses such as initiation stress, damage stress, and peak strength of hard and brittle marble under different confining pressures to provide a reference for the construction safety during underground rock mining and represents the other trend to research micro failure mechanism of rock besides the experiment carried out in the laboratory.

2 Triaxial numerical tests on marble

2.1 Establishment of numerical model

Based on the particle flow method, the numerical model was developed using PFC2D simulation software. Since the contact bond model can only transfer force, while the parallel bond model can transfer force and bending moment, it is more reasonable to use the parallel bond model to simulate the mechanical test of rock material [27–29].

In the parallel bond model, it is necessary to assign micromechanical parameters corresponding to the macroscopic parameters of the rock, so laboratory triaxial compression tests were conducted. The rock specimen was taken from the Jinping Grade II hydropower station and processed into a cylindrical model of 50 mm in diameter and 100 mm in height. The loading of the processed rock samples was controlled by displacement, and the confining pressure was set to 5, 10, and 15 MPa, and three tests were conducted under the same confining pressure.

The numerical tests were carried out based on laboratory triaxial compression tests of marble. The particle size of marble in nature generally ranged from 0.4 to 1.7 mm. The size of the numerical model is consistent with the size of the marble specimen, and the particle size ratio is 1.66 [30]. After several trial calculations, $L/R_{\rm min}$ was chosen to be 125, the minimum particle radius is 0.4 mm, and the number of particles was 4,943, which was a good fit. Based on the elastic modulus, peak strength, and peak strain of the marble rock sample, the mesoscopic parameters of the numerical model are repeatedly adjusted, and the final parameters are shown in Table 1.

2.2 Microscopic parameter verification

Numerical triaxial compression tests were carried out on the numerical models using DEM under three confining

Table 1: Micro-mechanical parameters of numerical model

Parameters	Values	Parameters	Values
Density (kg·m ⁻³)	2,700	Radius multiplier	1.0
Particle size ratio	1.66	Parallel bond modulus (GPa)	25.0
Minimum particle size (mm)	0.4	Parallel bond stiffness ratio	3.5
Particle contact modulus (GPa)	23.0	Parallel bond normal strength (MPa)	75.0
Particle contact stiffness ratio	3.5	Parallel bond shear strength (MPa)	63.0
Friction coefficient	0.4	_	_

pressures (5, 10, and 15 MPa) to investigate the reasonableness of the mesoscopic parameters.

Figure 1 shows the stress-strain curves of conventional triaxial compression laboratory tests under different confining pressures (5, 10, and 15 MPa).

Figure 2 shows the comparison of stress-strain curves in the laboratory test and numerical test. As seen in Figure 2, the trends of stress-strain curves are similar for the two tests under different confining pressures.

The macro mechanical parameters obtained from the laboratory tests and numerical tests under different confining pressures (5, 10, and 15 MPa) are shown in Table 2. From Table 2, it can be seen that the mechanical parameters obtained from both tests are similar.

Figure 3 shows the crack distribution of the marble under different confining pressures (5, 10, and 15 MPa) when the failure occurred in the laboratory and numerical simulation tests. It can be seen from Figure 3 that the final fracture surface morphology of both is a single fracture surface with diagonal, and the failure shape of marble is of shear failure. The width of the fracture zone increases with the confining pressure without obvious other fractures. Comparing stress-strain curves, macro-mechanical

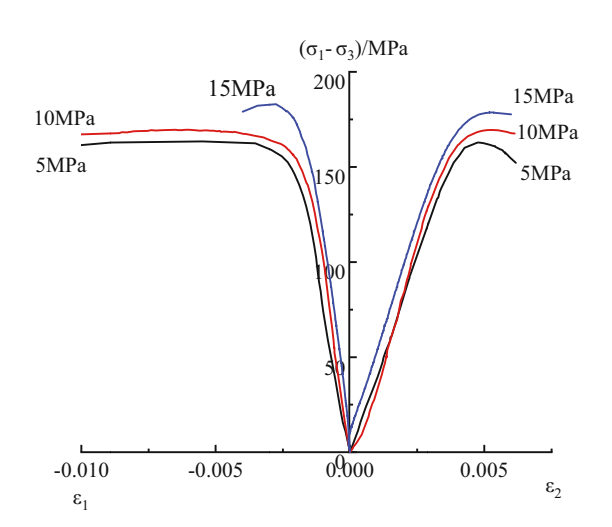
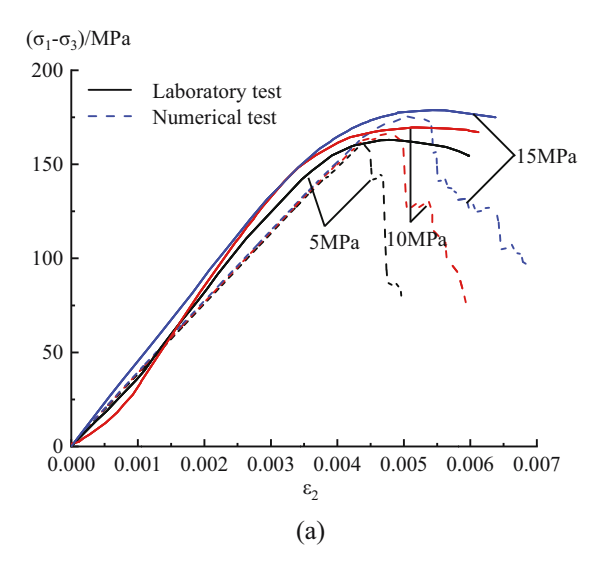


Figure 1: Stress-strain curves in conventional triaxial compression tests.

parameters, and damage forms of specimens in two tests shows that the mesoscopic parameters well reflect the macro-mechanical properties of marble.



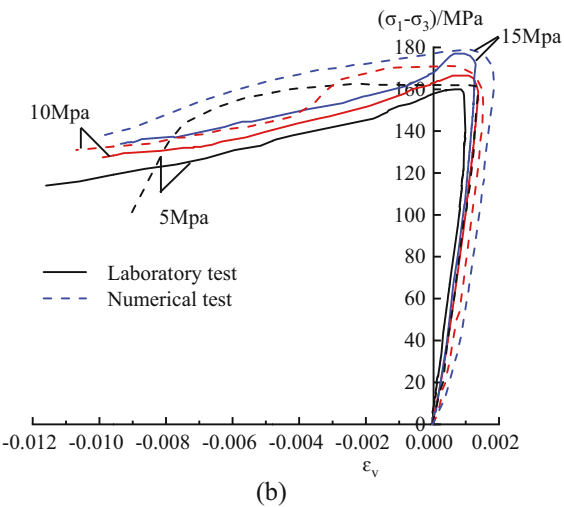


Figure 2: Stress strain curves. (a) Stress and axial strain curves and (b) stress and volume strain curves.

4 — Yan-Shuang Yang et al. DE GRUYTER

Fable 2: Mechanical parameters of marble and numerical model

Confining		Peak stress (MPa)	a)		Peak strain (%)		.	Elastic modulus (GPa)	iPa)
pressure (MPa)	Laboratory test	Numerical test	aboratory test Numerical test Relative error (%) Laboratory test Numerical test Relative error (%) Laboratory test Numerical test Relative error (%)	Laboratory test	Numerical test	Relative error (%)	Laboratory test	Numerical test	Relative error (%)
5	163.06	160.08	1.83	0.491	0.441	10.18	41.28	36.63	11.26
10	170.54	166.28	2.50	0.536	0.468	12.69	42.33	37.33	11.81
15	178.73	175.40	1.86	0.573	0.505	11.87	44.31	38.09	14.04

2.3 Triaxial compression numerical test under different loading rates

The loading rate is set to a low and stable value during the loading process to ensure that the specimen remains in quasi-static equilibrium throughout the test. The DEM model is in a dynamic mode controlled by Newton's second law, and the time step in each calculation cycle is a minimal value [31]. Loading is achieved by controlling the wall to move at a constant rate in opposite directions. Since the loading rate recommended in the PFC2D manual for the triaxial compression test is 0.02 m·s⁻¹, the loading rate selected for the parameter calibration is 0.02 m·s⁻¹. Apply lateral pressure and axial pressure to predetermined confining pressure at a loading speed of 0.02 m·s⁻¹. The confining pressure remains constant during the test. Converting the time step to the loading plate movement speed, it takes more than 100,000 steps to move the plate by 1 mm at 0.2 m·s⁻¹ loading rate, which satisfies the static loading requirement [32]. Based on the completion of the calibration, the loading rate interval of the indoor test was used as a reference and the numerical simulations with loading rates of 0.005, 0.01, 0.05, 0.1, 0.3, and $0.5 \,\mathrm{m\cdot s^{-1}}$ were designed to analyze the effect of loading rate on rock deformation and damage [33,34].

3 Numerical simulation tests under different loading rates

3.1 Effect of loading rate on the stress-strain curve

The stress–strain curves for the six loading rates under triaxial compression conditions under confining pressures of 5, 10, and 15 MPa are shown in Figure 4.

As shown in Figure 4, the numerical model under different loading rates has no compaction stage, and the stress–strain curve is divided into the elastic phase, plastic stage, and failure stage. The loading rate still affects the stress–strain curve. When the loading rate is lower than 0.1 m·s⁻¹, the stress–strain curve reaches its peak and then falls off rapidly, and the brittle characteristics of the rock sample occur. As the loading rate increases, the stress-strain decreases slowly in the post-peak phase, indicating that the ductile damage characteristics of the specimen become more pronounced at higher loading rates, which is consistent with the findings of Liu *et al.* [35].

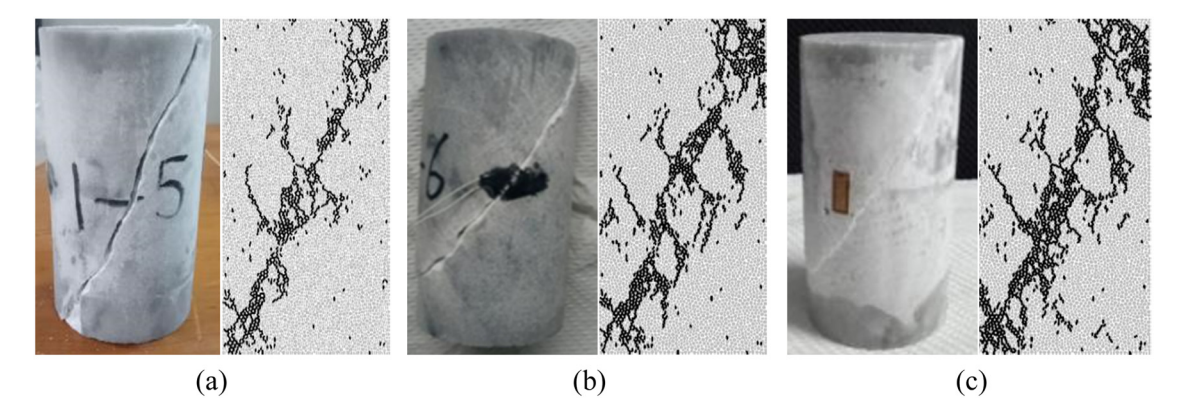


Figure 3: Failure characteristics. (a) 5 MPa, (b) 10 MPa, and (c) 15 MPa.

The peak strength and strain of marble increased with the increase in loading rate under the same confining pressure. When the confining pressure varies from 5 to 15 MPa, the effect of loading rate on the peak strength of marble increases with the increase in confining pressure. When the loading rate increased from 0.005 to 0.5 m·s⁻¹ under 5 MPa confining pressure, the peak strength increased from 159.6 to 171.2 MPa accordingly, and the increase was 7.30%. The peak strength of marble increased from 174.5 to 191.1 MPa when the rate was increased from 0.005 to 0.5 m·s⁻¹ at 15 MPa, and the increase in peak strength was 9.52%.

3.2 Effect of loading rate on strength parameters

In geotechnical engineering, the Mohr-Coulomb strength criterion can characterize the "ultimate equilibrium condition" between the stresses at the time of imminent damage and determine whether the rock will be damaged under the current stress state. According to the Mohr-Coulomb strength criterion, the cohesion and the angle of internal friction are obtained. The relationship between the values of the strength parameters and the loading rate is shown in Figure 5. From Figure 5, it can be seen that the cohesion and internal friction angle are linearly related to the loading rate when the loading rate ranges from 0.005 to 0.5 m·s⁻¹. The cohesion and internal friction rise of the marble increase with the increase in the loading rate. The correlation coefficients of cohesion and internal friction angle with the loading rate were 0.996 and 0.971, respectively, indicating that the two strength parameters were highly correlated with the loading rate. The strength parameters change significantly under high loading rate, which indicates that the rock samples are highly fragmented under high loading rate and the frictional effect between the particles is obvious.

3.3 Effect of loading rate on characteristic stress

The compressive damage process of the rock is divided into stages. The three steps of the stress–strain curve correspond to the characteristic stresses of initiation stress, damage stress, and peak stress. According to the research results of Zhu *et al.* [36–38], the stress value corresponding to the first appearance of microcrack in PFC was selected as the initiation stress. The inflection point of the volume strain curve and the peak point of the stress–strain curve was taken as the damage stress and peak stress. Take the loading rate of 0.005 m·s⁻¹ under 10 MPa confining pressure as an example, as shown in Figure 6. Among them, the volumetric strain is calculated as follows:

$$\varepsilon_{v} = 2\varepsilon_{1} + \varepsilon_{2},$$
 (1)

where ε_1 is the circumferential strain and ε_2 is the axial strain

Figure 7 shows the analysis of the characteristic stress of marble under different confining pressures (5, 10, and 15 MPa) about the loading rate. From Figure 7, it can be seen that the characteristic stress of marble gradually increases with the increase in loading rate, and there is an apparent positive correlation between the characteristic stress and the loading rate. Under the same confining pressure, the growth rate of the peak strength increases faster with the speed increase when the rate range is 0.005–0.5 m·s⁻¹. The loading rate has the most significant effect on peak strength compared to initiation stress and damage stress. The correlation between the loading rate and the peak strength was higher than 0.99 for different confining pressures, consistent with the findings of Zheng et al. [39]. When the confining pressure increases, the expansion of marble at the same loading rate requires higher stress. The overall initiation and damage stress level

6 — Yan-Shuang Yang et al. DE GRUYTER

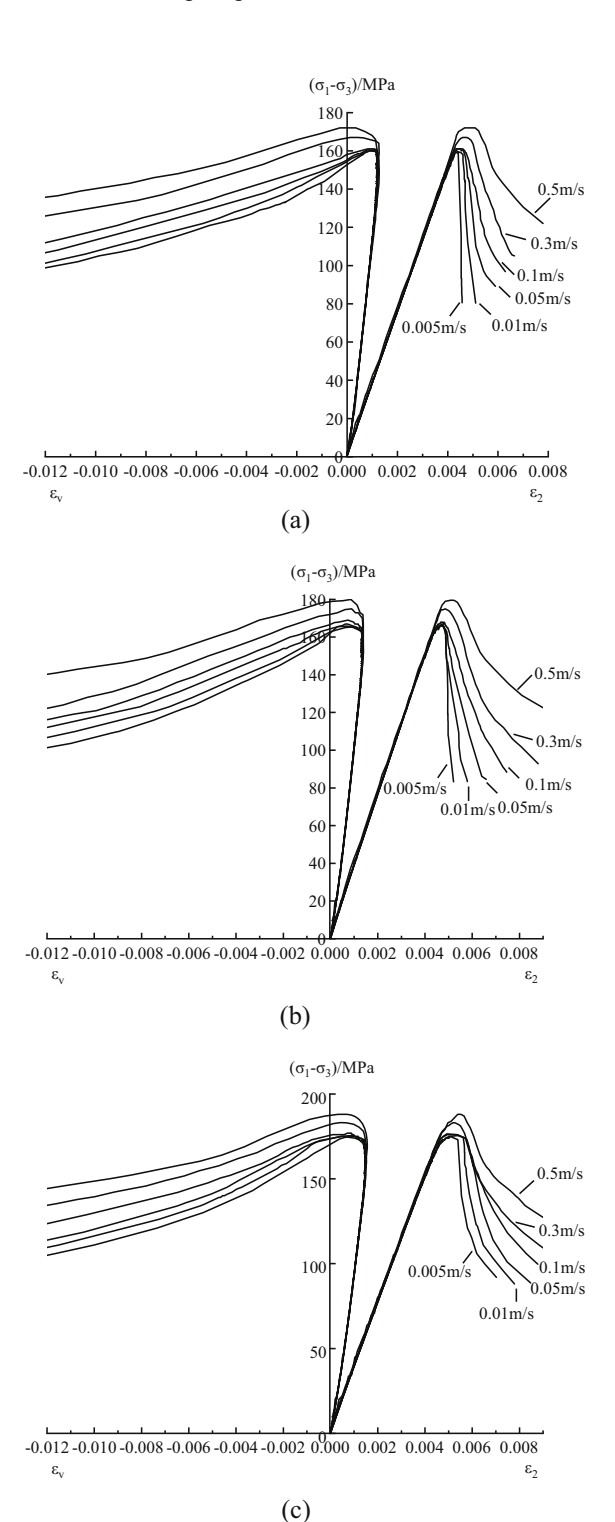


Figure 4: Stress–strain curves for different loading rates. (a) 5 MPa, (b) 10 MPa, and (c) 15 MPa.

is increased accordingly, and the growth is more significant at lower rates. When the loading rate was $0.005\,\mathrm{m\cdot s^{-1}}$, the rise of initiation and damage stress was 4.76 and 23.48%, and the increase was reduced to 2.94 and 11.14%,

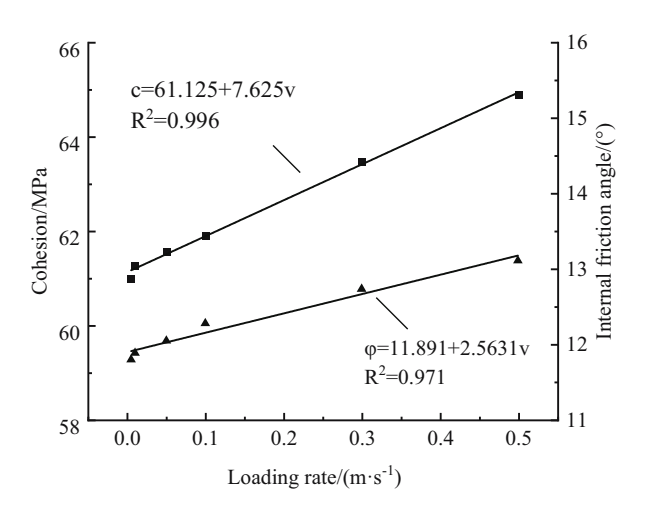


Figure 5: Relationship between strength parameters and loading rates.

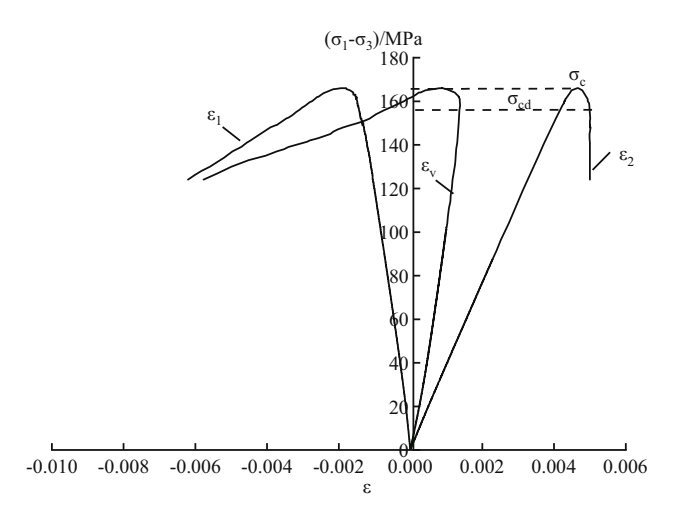


Figure 6: Stress–strain curve of the specimen at a loading rate of $0.005~\text{m}\cdot\text{s}^{-1}$.

respectively, when the loading rate was $0.5 \,\mathrm{m\cdot s^{-1}}$. Confining pressure has a suppression effect on the specimen's deformation. The effect of confining pressure on the peak stress is more significant at a high-speed rate. The peak stress increase is 6.66% when the loading rate is at the interval minimum $(0.005 \,\mathrm{m\cdot s^{-1}})$ and 11.60% at the interval maximum loading rate $(0.5 \,\mathrm{m\cdot s^{-1}})$ by increasing the confining pressure.

3.4 Effect of loading rate on crack development

The final damage pattern of the specimens under different confining pressures and loading rates in the numerical simulation test is shown in Figure 8. As seen from Figure 8,

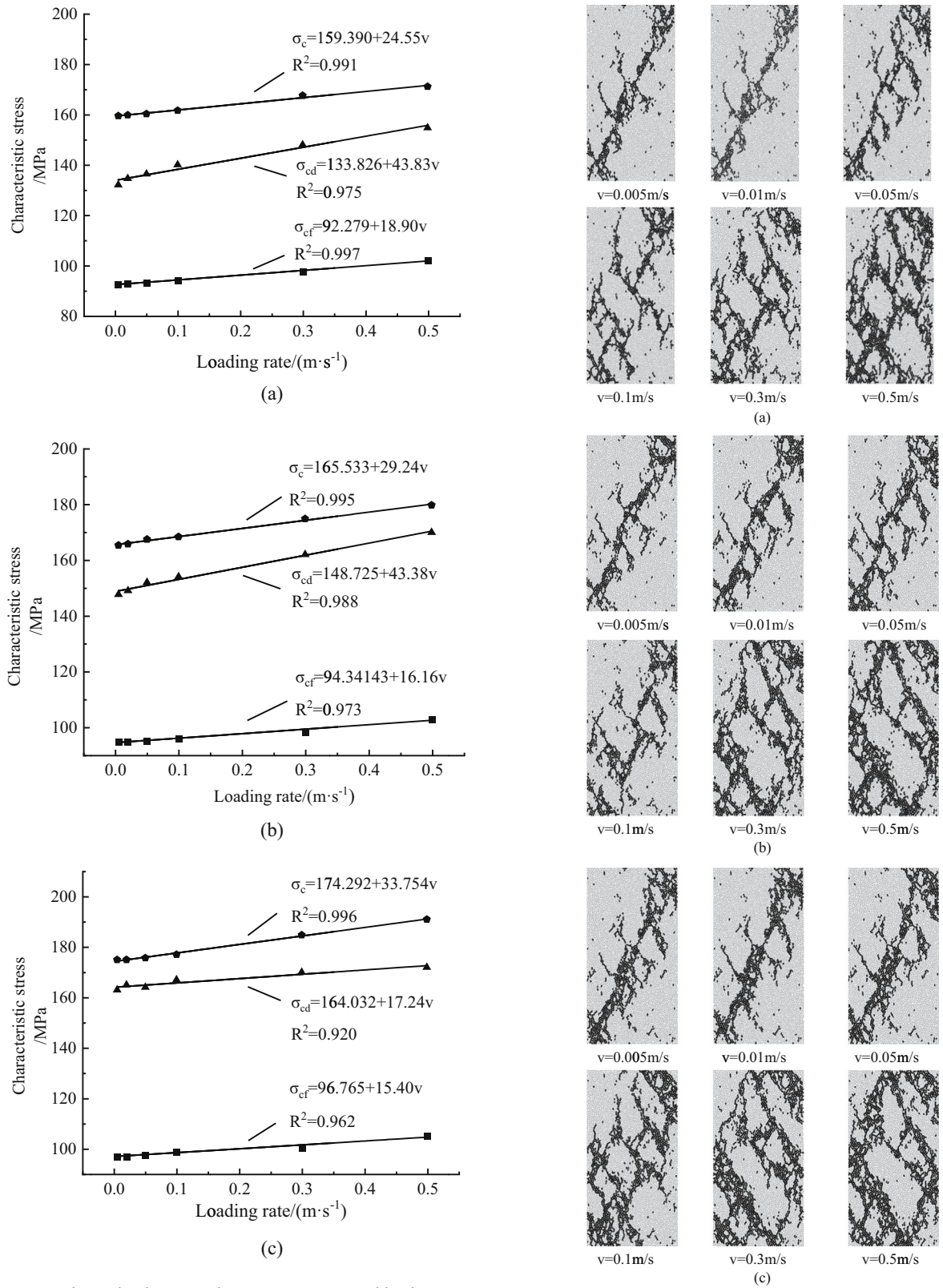
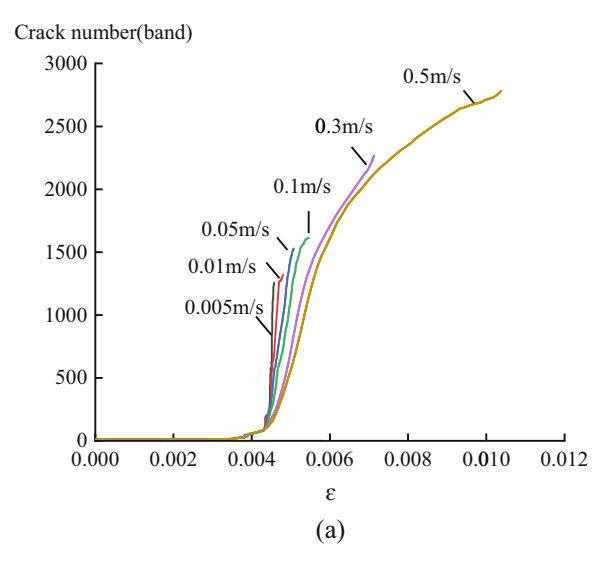
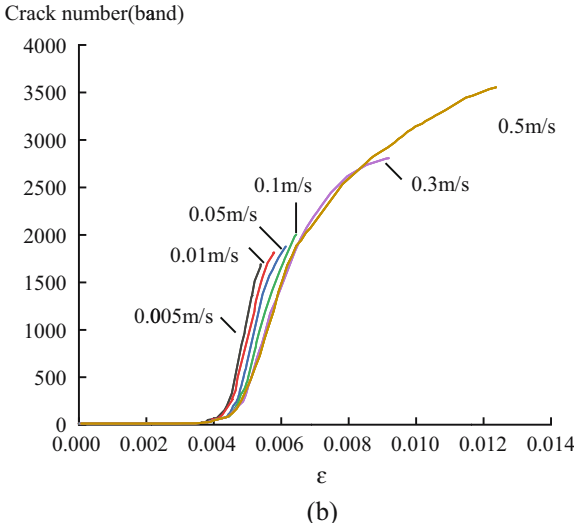


Figure 7: Relationship between characteristic stress and loading rates. (a) 5 MPa, (b) 10 MPa, and (c) 15 MPa.

Figure 8: Failure characteristics. (a) 5 MPa, (b) 10 MPa, and (c) 15 MPa.

8 — Yan-Shuang Yang et al. DE GRUYTER





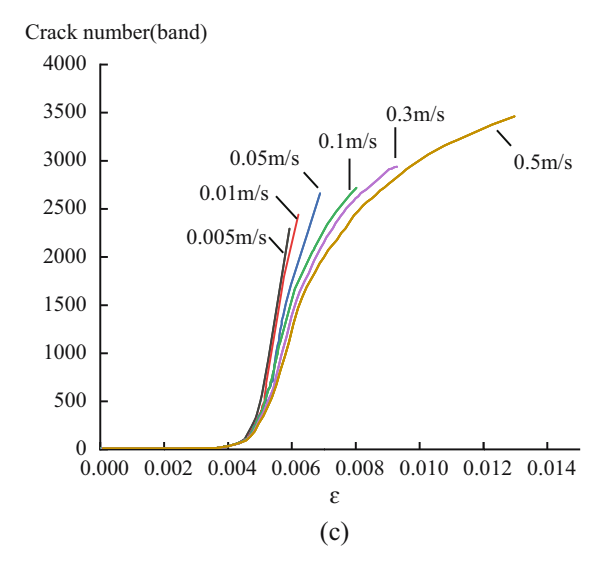


Figure 9: Micro-crack number evolution curves. (a) 5 MPa, (b) 10 MPa, and (c) 15 MPa.

when the loading rate takes the value interval from 0.005 to 0.05 m·s⁻¹, the diagonal oblique cracks are produced on the surface of the marble when it is damaged, and the damage form is a shear failure. With the increase in the loading rate of 0.1–0.5 m·s⁻¹, the internal microcracks of marble changed from being concentrated on both sides of the diagonal cracks to uniformly distributed inside the rock sample, and more cracks appeared at the top and bottom of the specimen as well. The fragmentation degree of rock samples at high loading rates was significantly higher than that at other low loading rates [40]. Shear failure along the diagonal no longer occurred in rock samples [41]. The form of destruction appeared significantly different from that at low rates, which is consistent with the conclusion of the relevant study by Li *et al.* [27,42].

The number of cracks throughout the loading was recorded by compiling the FISH code to obtain the variation in the number of cracks with axial strain in the numerical test of triaxial compression of marble. The curves of the number of cracks vs strain inside the marble under different loading rates are shown in Figure 9. From Figure 9, it can be seen that the total number of cracks increases exponentially with the increase in loading rate, and the axial deformation when cracks appear in the rock samples at different rates is approximately the same. In the numerical experiments, monitoring stops when the rock sample breaks. As the loading rate increases, the strength of the rock increases, requiring greater deformation to cause the overall destruction of the rock sample, and therefore the strain at the crack monitoring cutoff is greater. The total number of cracks generated by loading under different confining pressures increases with the increase in the loading rate. This is because at higher loading rates, both compressive strength and axial strain rise. The number of microcracks gradually increases with the increase in the loading rates. At the same time, the surrounding pressure limits the lateral deformation of the rock sample and slows down the accumulation rate of rock damage, so the increase is slowed down accordingly. When the rate was increased from 0.005 to 0.5 m·s⁻¹, the total number of cracks generated by the loading process increased by 122% at a confining pressure of 5 MPa and 30.2% at a confining pressure of 15 MPa.

Figure 10 shows the variation curves of the number of tensile cracks and shear cracks with loading rate under different confining pressures. Considering that the total number of cracks in each numerical test is different, the total number of cracks at the peak point and the total number of cracks at the time of failure are normalized. It can be seen from Figure 10 that with the increase in the confining pressure, the proportion of shear cracks in the

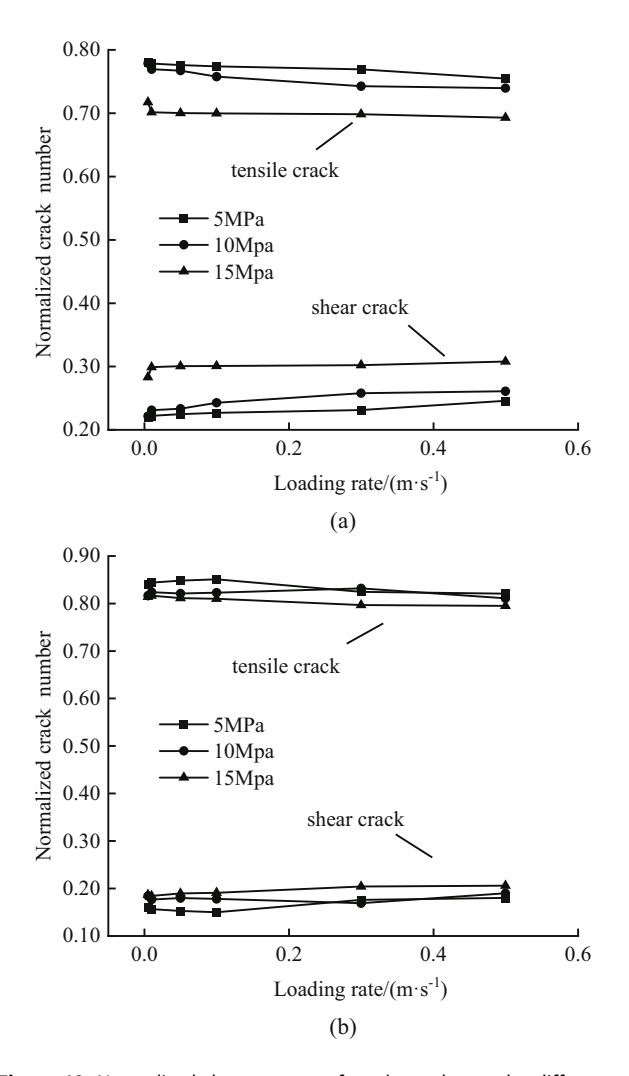


Figure 10: Normalized change curve of crack number under different confining pressures. (a) At peak stress and (b) at failure.

specimen increases at different rates. When the confining pressure is high, the microcrack closing pressure increases and the crack propagation is limited. The number of tensile cracks gradually decreases, and the number of shear cracks gradually increases. It can be seen from Figure 10(b) that under the same confining pressure, with the increase in loading rate, the curve fluctuates up and down within a certain range, but it is not obvious, which indicates that the number of normalized tensile cracks and shear cracks on the final failure surface of the specimen under same confining pressure are basically the same.

4 Conclusion

Numerical triaxial compression tests were conducted on marble under different confining pressures based

on laboratory tests combined with DEM models. The loading rate effect of hard brittle marble under conventional confining pressure was investigated by monitoring and recording rock specimens' stress-strain curves, crack numbers, and characteristic stress changes throughout the loading process. The experimental results were compared and verified with the results of existing related studies to obtain the effect of different loading rates on the deformation and damage of hard brittle rocks in triaxial compression tests. By adjusting the excavation rate and supporting reinforcement measures, the threat of engineering hazards caused by excavation can be effectively controlled. The following conclusions are drawn:

1) The transformation from brittle failure to ductile failure occurs in hard brittle marble at different loading rate within the range of 0.005–0.5 m·s⁻¹, and this transformation gradually becomes less evident with increasing confining pressure.

2) A significant linear relationship exists between characteristic stress and loading rate, all positively correlated. The peak strength has the highest positive correlation with the loading rate, and there is a significant enhancement effect of high-speed loading on the rock strength. When the rate level increases from the minimum value (0.005 m·s⁻¹) to the maximum value (0.5 m·s⁻¹) in the interval, with the increase in confining pressure, the increase ratio of peak stress correspondingly increases from 6.66 to 11.60% accordingly. The increase in the confining pressure will weaken the dependence of each characteristic stress on the loading rate.

3) Under the same confining pressure, the faster the loading rate, the later the crack generation, the higher the crack initiation stress, and finally, the damage appears. The increase in the number of cracks was reduced from 122 to 30.2% by increasing the loading rate when the confining pressure was increased from 5 to 15 MPa.

Acknowledgments: The authors thank the National Natural Science Foundation of China (Nos 51609080 and 51708188) and the Hubei Key Research and Development projects (No. 021BAA050). The authors also express sincere gratitude to the editor and reviewers for their valuable comments, which have greatly improved this article.

Funding information: This research was granted by the National Natural Science Foundation of China (Nos 51609080 and 51708188) and the Hubei Key Research and Development projects (No. 021BAA050).

Author contributions: Yang: conceptualization and methodology; Yin, Cheng, and Hou: validation and investigation; and Zhang: supervision.

Conflict of interest: The authors state no conflict of interest.

Data availability statement: The data supporting this study's findings are available from the corresponding author upon reasonable request.

References

- [1] Dong, L. L., L. Peng, Y. H. Li, T. S. Zhao, Y. P. Sun, P. W. Xiao, et al. Mechanical response and stability analysis of surrounding rock mass during roof arch excavation of high stress underground powerhouse. *Chinese Journal of Rock Mechanics and Engineering*, Vol. 42, 2023, pp. 1–14.
- [2] Fan, Q. X., Z. L. Wang, H. Wei, L. Peng, H. B. Wang, J. R. Xu, et al. Technological innovations in construction of underground caverns in basaltic rocks at Baihetan Hydropower Station on Jinsha River. *Scientia Sinica (Technological)*, Vol. 51, No. 9, 2021, pp. 1088–1106.
- [3] Li, B., Q. F. Ding, N. W. Xu, Y. F. Lei, Z. P. Zhu, and J. F. Liu. Mechanical response and stability analysis of rock mass in high geostress underground powerhouse caverns subjected to excavation. *Journal of Central South University*, Vol. 2710, 2020, pp. 2971–2984.
- [4] Zhao, J., G. T.Guo, D. P. Xu, X. Huang, C. Hu, Y. L. Xia, et al. Experimental study of deformation and failure characteristics of deeply-buried hard rock under triaxial and cyclic loading and unloading stress paths, *Rock and Soil Mechanics*, Vol. 41, No. 5, 2020, pp. 1521–1530.
- [5] Feng, Z. Z. and Y. X. Shen. Study on precursor identification of rock instability based on surface displacement. *Chinese Journal of Rock Mechanics and Engineering*, Vol. 40, No. S2, 2021, pp. 3024–3032.
- [6] Li, H. Y., X. H. Liu, Y. Zheng, and W. G. Xiao. Analysis of characteristic energy during the progressive failure of deep-buried marble in Jinping. *Chinese Journal of Rock Mechanics and Engineering*, Vol. 40, No. S2, 2022, pp. 3229–3239.
- [7] Ding, X. L., Y. T. Zhang, S. L. Huang, J. J. Chi, C. J. Zhang, and D. X. Deng. Large deformation mechanism of surrounding rock masses of tunnels, prediction method of squeezing large deformation and its application. *Chinese Journal of Rock Mechanics and Engineering*, Vol. 42, No. 3, 2023, pp. 521–544.
- [8] Yang, Y. S., H. Zhou, S. H. Mei, Z. R. Zhang, and J. L. Li. A case study of the excavation damage zone expansion time effect in hard brittle country rock under high geostress: characteristics and mechanism. *Rock and Soil Mechanics*, Vol. 41, No. 4, 2020, pp. 1357–1365.
- [9] Jiang, D. Y., Z. Y. Yang, J. Y. Fan, Z. Z. Li, J. J. Suo, and J. Chen. Experimental study of load rate effect of salt rock during loading and unloading. *Rock and Soil Mechanics*, Vol. 44, No. 2, 44, 2023, pp. 403–414.
- [10] Yang, Y. S., M. Y. Ying, S. P. Cheng, and J. W. Hou. The effect of loading rate of granite under confining pressure based on particle flow simulation. *Water Resources and Power*, Vol. 40, No. 10, 2022, pp. 170–172.
- [11] Liang, Z. Z., X. K. Qian, Y. F. Zhang, and Z. Y. Liao. Numerical simulation of dynamic fracture properties of rocks under different static stress conditions. *Journal of Central South University*, Vol. 29, No. 2, 2022, pp. 624–644.

- [12] Zhou, H., Y. S. Yang, H. B. Xiao, C. Q. Zhang, and Y. P. Fu. Research on loading rate effect of tensile strength property of hard brittle marble-test characteristics and mechanism. *Chinese Journal* of Rock Mechanics and Engineering, Vol. 32, No. 9, 2013, pp. 1868–1875.
- [13] Meng, Q. B., L. J. Han, H. Pu, S. Y. Wen, and H. Li. Experimental on the effect of strain rate and size on the energy accumulation and dissipation of rock. *Journal of China Coal Society*, Vol. 40, No. 10, 2015, pp. 2386–2398.
- [14] Jiang, D. Y., K. N. Xie, X. Jiang, J. Chen, and X. Yuan. Statistical analysis of acoustic emission energy distribution during uniaxial compression of shale. *Chinese Journal of Rock Mechanics and Engineering*, Vol. 35, No. S2, 2016, pp. 3822–3828.
- [15] Qin, T., X. Guo, Y. L. Huang, Z. X. Wu, W. Y. Qi, and H. Wang. Study on macro-meso deformation law and acoustic emission characteristics of granular gangue under different loading rates. *Minerals*, Vol. 2, No. 11, 2022, pp. 1422–1435.
- [16] Zhao, K., X. Yu, Y. Zhou, Q. Wang, J. X. Wang, and J. L. Hao. Energy evolution of brittle granite under different loading rates. *International Journal of Rock Mechanics and Mining Sciences*, Vol. 132, 2020, id. 104392.
- [17] Li, S. G., G. F. Chen, H. Q. Shuang, H. F. Lin, and P. X. Zhao. Experimental study on effect of loading rate and initial damage on energy evolution of sandstone. *Journal of Mining & Safety Engineering*, Vol. 36, No. 2, 2019, pp. 373–380.
- [18] Tian, W. Q., S. Q. Yang, and G. Fang. Particle flow simulation on mechanical behavior of coal specimen under triaxial cyclic loading and unloading. *Journal of China Coal Society*, Vol. 41, No. 3, 2016, pp. 603–610.
- [19] Zhang, Y., Z. Q. Ding, C. Fang, and B. T. Cong. Three-dimensional particle flow simulation on macro-micro mechanical properties of granite under triaxial cyclic loading and unloading. *Mining Research* and Development, Vol. 39, No. 4, 2019, pp. 52–58.
- [20] Shi, C., Q. Zhang, and S. N. Wang. Numerical Simulation Technology and Application with Particle Flow Code (PFC5.0). China Architecture and Building Press, Beijing, 2018.
- [21] Cundall, P. A. and O. D. L. Strack. A discrete numerical model for granular assemblies. Géotechnique, Vol. 29, No. 1, 1979, pp. 47–65.
- [22] Francois., N., L. Sibille, F. Donze, and F. Darve. From microscopic to macroscopic second-order work in granular assemblies. *Mechanics* of *Materials*, Vol. 39, No. 7, 2007, pp. 664–684.
- [23] Guo, J. J. and X. Y. Cheng. Test of Crack Evolution of Coal Samples Under Cyclic Loading and Numerical Simulation. Safety in Coal Mines, Vol. 50, No. 9, 2019, pp. 71–74.
- [24] Hong, J. T. and M. Xu. DEM study on the undrained mechanical behavior of gassy sand. *Acta Geotechnica*, Vol. 15, No. 8, 2020, pp. 2179–2193.
- [25] Kim, E., M. A. Stine, and D. B. M. D. Oliveira. Effects of water content and loading rate on the mechanical properties of Berea sandstone. *Journal of the Southern African Institute of Mining and Metallurgy*, Vol. 119, No. 12, 2019, pp. 1077–1082.
- [26] Zhou, E. K., Z. C. Wang, H. Chen, W. Q. Zhang, and X. B. Wu. Effects of loading rate on macroscopic and mesoscopic mechanical properties of sandstone. *Chinese Journal of Underground Space and Engineering*, Vol. 16, No. S2, 2020, pp. 647–655.
- [27] Zhang, Y. and J. T. Li. Study on fracture characteristics of marble under monotone and cyclic loading. *Chinese Journal of Rock Mechanics and Engineering*, Vol. 38, No. S2, 2019, pp. 3313–3320.
- [28] Sun, C., Y. H. Ao, J. M. Zhang, and S. Wang. Particle flow of mesofracture characteristics and macro-scale effect of granites. *Chinese*

- *Journal of Geotechnical Engineering*, Vol. 42, No. 9, 2020, pp. 1687–1695.
- [29] Liu, J. and J. T. Li. Analysis on meso-damage characteristics of marble under triaxial cyclic loading and unloading based on particle flow simulation. *Journal of Central South University (Science and Technology)*, Vol. 9, No. 11, 2018, pp. 2797–2803.
- [30] Hao, B. Q., C. S. Zhang, C. L. Wang, and C. Ren. Study on determination of micro-parameters of rock PFC2D model. *Coal Science and Technology*, Vol. 50, No. 4, 2022, pp. 132–141.
- [31] Cheng, P. Y. Loading rate effect analysis on rock particle flow model under uniaxial compression. *Chinese Journal of Underground Space* and Engineering, Vol. 14, No. 3, 2018, pp. 635–642.
- [32] Cho, N., C. D. Martin, and D. C. Sego. A clumped particle model for rock. *International Journal of Rock Mechanics and Mining Sciences*, Vol. 44, No. 7, 2007, pp. 997–1010.
- [33] Wang, X. D. and K. Wang. Effect of loading rate on mechanical properties and energy conversion mechanism of granite fracture. Safety in Coal Mines, Vol. 51, No. 4, 2020, pp. 31–35.
- [34] Ma, L. J., B. Xue, D. R. Wang, C. Zhou, and S. Y. Luo. Loading rate effect on shear strength and deformation properties of salt rock. *Journal of Basic Science and Engineering*, Vol. 30, No. 4, 2022, pp. 1039–1047.
- [35] Liu, X. H., Y. Zheng, Q. J. Hao, X. Gui, and Y. Xue. Brittleness characteristics of quasi-static triaxial coal rock based on characteristic stress. *Chinese Journal of Rock Mechanics and Engineering*, Vol. 40, No. 12, 2021, pp. 2454–2465.

- [36] Zhu, J., J. H. Deng, Y. M. Huang, T. Liu, and Y. J. Ma. Study of loading rate effect on characteristic stresses of marble. *Journal of Harbin Institute of Technology*, Vol. 52, No. 2, 2020, pp. 75–81.
- [37] Liu, X. H., X. Gui, J. Yu, Q. J. Hao, and X. P. Zhao. Dilatancy characteristics and crack evolution of deep-buried marble under unloading confining pressure. *Chinese Journal of Underground Space and Engineering*, Vol. 18, No. 6, 2022, pp. 1922–1932.
- [38] Hou, Z. Q., Y. Wang, D. Q. Liu, and C. H. Li. Investigation of the anisotropic mechanical behaviors and energy evolution of interbedded marble. *Journal of Mining & Safety Engineering*, Vol. 36, No. 4, 2019, pp. 794–804.
- [39] Zheng, H. H., Z. Q. Ma, L. Zou, D. Y. Zhang, and X. C. Liu. Effect of loading rate and confining pressure on strength and energy characteristics of mudstone under pre-cracking damage. *Energies*, Vol. 15, No. 10, 2022, pp. 1–15.
- [40] Yin, X. T., X. R. Ge, C. G. Li, and S. L. Wang. influences of loading rates on mechanical behaviors of rock materials. *Chinese Journal of Rock Mechanics and Engineering*, Vol. 29, No. S1, 2010, pp. 2610–2615.
- [41] Yu, L. Q., Q. L. Yao, Q. Xu, W. N. Wang, Z. J. Niu, and W. D. Liu. Experimental and numerical simulation study on crack propagation of fractured fine sandstone under the influence of loading rate. *Journal of China Coal Society*, Vol. 4611, 2021, pp. 3488–3501.
- [42] Li L. F., H. L. Deng, X. H., Zhang, and L. P. Han. Experimental study on the effect of loading rate on triaxial mechanical properties of real-time high temperature granite. *Science Technology and Engineering*. Vol. 20, No. 16, 2020, pp. 6397–6403.